npj | climate and atmospheric science

www.nature.com/npjclimatsci

ARTICLE OPEN

Check for updates

Combined influences of sources and atmospheric bleaching on light absorption of water-soluble brown carbon aerosols

Wenzheng Fang[1,2]✉, August Andersson[2], Meehye Lee[3], Mei Zheng[4], Ke Du[5], Sang-Woo Kim[6], Henry Holmstrand[2] and Örjan Gustafsson[2]✉

Light-absorbing Brown Carbon (BrC) aerosols partially offset the overall climate-cooling of aerosols. However, the evolution of BrC light-absorption during atmospheric transport is poorly constrained. Here, we utilize optical properties, ageing-diagnostic δ^{13}C-BrC and transport time to deduce that the mass absorption cross-section ($MAC_{WS\text{-}BrC}$) is decreasing by ~50% during long-range oversea transport, resulting in a first-order bleaching rate of 0.24 day^{-1} during the 3-day transit from continental East Asia to a south-east Yellow Sea receptor. A modern ^{14}C signal points to a strong inverse correlation between BrC light-absorption and age of the source material. Combining this with results for South Asia reveals a striking agreement between these two major-emission regions of rapid photobleaching of BrC with a higher intrinsic absorptivity for BrC stemming from biomass burning. The consistency of bleaching parameters constrained independently for the outflows of both East and South Asia indicates that the weakening of BrC light absorption, thus primarily related to photochemical processes rather than sources, is likely a ubiquitous phenomenon.

npj Climate and Atmospheric Science (2023)6:104 ; https://doi.org/10.1038/s41612-023-00438-8

INTRODUCTION

Bottom-up emission inventories (EI) estimate that black carbon (BC) and organic carbon (OC) emissions from Asia contribute ~45% and 24% of global emissions, respectively[1]. This carbon aerosol pollution arises from a poorly resolved mixture of anthropogenic sources such as traffic, industry, wildfires and residential combustion of solid fuels[1,2]. The resulting atmospheric brown clouds are warming the atmosphere yet dimming the surface over these vast regions, severely impacting air quality, health and climate[3–5]. The climate effects of aerosols are more complex than the warming effects of CO_2 and other greenhouse gases and dominate the uncertainty associated with the total anthropogenic impact on climate change[2–4,6]. Organic aerosols (OA) are well-known as light-scattering particles. However, studies are increasingly showing that a fraction of OA also appreciably absorbs solar radiation; this fraction is referred to as BrC[7,8]. Some estimates imply that BrC plays an important role in counteracting the general cooling effect of other scattering aerosols. Yet, its contribution to climate forcing is poorly constrained[9,10] and, therefore, not yet quantitatively considered in the overall radiative forcing estimates of the IPCC[6].

A number of investigations of the light absorption of OA formed from laboratory-based fuel burning and wildfires plume suggest that both biomass burning (BB) and some fossil fuel burning could yield BrC (e.g., refs. [11–19]). The BrC absorptivity displays high variability and likely depends on a combination of combustion conditions (e.g., temperature, air-to-fuel ratio, stove construction), combustion efficiency and fuel types[11–13,18,19]. However, the relationship between the relative source contributions to BrC and BrC absorption remains to be understood.

The photochemical ageing after emission impacts the light absorption properties of BrC in the ambient atmosphere. Laboratory[12,14,16,18–21] and wildfire plume[15] studies found a rapid degradation of BrC absorptivity through photochemical bleaching processes. However, the magnitude and exact bleaching processes in fire emissions and the real atmosphere are highly uncertain[7,8,13,15,18–24]. In addition to primary emissions, secondary OA (SOA) formation in smog chambers[13,18,20,25,26] and wildfire plumes[23,27,28] was surmised to contribute to BrC. But other field measurements suggested little to no net change in SOA in wildfire plumes[15,29–31], and its absorption instead showed decay[15,32]. The SOA (or secondary BrC) to total OA (or BrC) and evolution of BrC has remained elusive in part because it is challenging to separate the amount of SOA (or secondary BrC) quantitatively and thus the absorption of SOA (or secondary BrC) from the primary, secondary and ageing processes. The combined larger uncertainties in BrC's EI, optical properties and fate make it difficult for models to predict the BrC dynamics and influence on the overall aerosol–climate effects, thus calling for more observational constraints[33,34].

A large fraction of OC is water-soluble (WSOC; ~30 to 80% of OC in Asia)[7,35–43] and atmospherically transformable[7,35,37,39,40,43]. The WSOC (mass analogue isolate of WS-BrC; hereafter, WS-BrC is used for WSOC) exhibits stronger wavelength dependence than BC and absorbs primarily at short visible and UV wavelengths[36–45]. Carbon isotopes (^{14}C, or ^{13}C (ref. [39])) were combined with optical measurements to investigate the light absorption and atmospheric processing of WS-BrC, e.g., in source areas[40] and regional receptor sites[37,43] in S. Asia, as well as in source area[46] and ocean background site in E. Asia[36]. However, these past optical observations of WS-BrC focused on either one site or similar source regimes, hampering our further understanding of the combined influences of sources and atmospheric processes during source-to-receptor transport in different regimes.

[1]Key Laboratory of Geographic Information Science, Ministry of Education, School of Geographic Sciences, East China Normal University, Shanghai 200241, China. [2]Department of Environmental Science (ACES) and Bolin Centre for Climate Research, Stockholm University, Stockholm 10691, Sweden. [3]Department of Earth and Environmental Sciences, Korea University, Seoul 02841, South Korea. [4]College of Environmental Sciences and Engineering, Peking University, Beijing 100871, China. [5]Department of Mechanical and Manufacturing Engineering, University of Calgary, Calgary T2N 1N4, Canada. [6]School of Earth and Environmental Sciences, Seoul National University, Seoul 08826, South Korea. ✉email: wzfang@geo.ecnu.edu.cn; orjan.gustafsson@aces.su.se

Taken together, atmospheric processes like oxidation, fuel types and fuel conditions consumed by burning, are surmised to impact the WS-BrC absorption, complicating bottom-up efforts to quantify and predict aerosol emission and its absorption properties[4,6,9–13,18,21,40]. Furthermore, there is limited use of combined optical and source-plus-process-diagnostic isotope techniques to diagnose the link between optical properties, sources, and atmospheric processes of WS-BrC in the large-emission region in E. Asia[36,46]. It remains incompletely understood to what extent the fuel sources (e.g., fossil vs. biomass) and atmospheric processing (e.g., photochemical ageing, decay and SOA) during source-to-receptor transport in key emission regions (e.g., E. and S. Asia) could influence the WS-BrC optical properties[7,36,37,39,46], causing difficulties in modelling and mitigating the regional climate impact of WS-BrC.

Here we combined the optical properties and radiocarbon $^{14}C/^{12}C$ and stable carbon $^{13}C/^{12}C$ signatures of WS-BrC to deduce its emission sources-impacted light-absorbing properties and the dynamically changing absorptivity of WS-BrC during source-to-receptor transport for the 2014 East Asian regional haze campaign. The ^{14}C signatures allow quantitatively calculating the fraction of fossil versus biomass in different regions (e.g., E. and S. Asia)[35–37,40,43,47–49]. In addition to ^{14}C, the $\delta^{13}C$ signature is a useful proxy tracing WS-BrC evolution[35] and photo-degradation[39] during source-to-receptor transport. Thus, the concurrent dual-isotope measurements provide both source fingerprints and information on stable-isotope-fractionating atmospheric transformations.

The $PM_{2.5}$ samples were collected simultaneously during the winter period (January 2014) from the representative hotspot regions of BrC emissions in E. Asia, including in the Beijing-Tianjin-Hebei (BTH) area, Yangtze River Delta (YRD), Pearl River Delta (PRD), Sichuan (SC) province and a large footprint SE Yellow Sea regional receptor site—the Korea Climate Observatory at Gosan (KCOG) (Fig. 1a; Supplementary Note 1 for detailed site information). The optical results are discussed and interpreted in terms of intrinsic carbon-isotope signatures, which reflect both sources and atmospheric processing. The evolution of mass absorption cross-section ($MAC_{WS\text{-}BrC}$) with ageing-tracing $\delta^{13}C_{WS\text{-}BrC}$ between the source area and the downwind receptor in East Asia is detailed to resolve the extent of atmospheric effects on absorption properties of WS-BrC. This is then combined with similar recently published data for S. Asia to explore commonality in WS-BrC ageing processes in these two very different, yet high-emissions, meteorological systems. We further combine the current E. Asian observations with earlier data in S. Asia, synthesizing findings between the two different regions and bridging the influence of sources and atmospheric processes on the light absorption of Asian water-soluble BrC with numerical simulations and conceptual models.

RESULTS

Meteorological conditions and regional aerosol regimes

High loadings of aerosols blanketed a large area of E. Asia during January 2014 (Fig. 1a). The regional-scale meteorological patterns showed that aerosol loadings at SC and PRD were influenced by southerly/southwesterly winds formed by an anticyclonic system over southern China. Beijing, BTH, Shanghai, YRD and KCOG were instead significantly influenced by prevailing northwesterly winds as indicated by the wind vectors in Fig. 1a. In line with the AOD map, the ground $PM_{2.5}$ levels in this campaign were observed to be consistently high in the four hotspot emission regions of China, with the highest values at BTH ($210 \pm 84\ \mu g\ m^{-3}$), followed by SC ($135 \pm 52\ \mu g\ m^{-3}$), PRD ($122 \pm 48\ \mu g\ m^{-3}$) and YRD ($92 \pm 53\ \mu g\ m^{-3}$) (Supplementary Table 1, Supplementary Figs. 1 and 2a). For $PM_{2.5}$ concentrations in the outflow of E. Asia (KCOG), there was a wide range with a minimum hourly concentration near $10\ \mu g\ m^{-3}$, with a maximum approaching $170\ \mu g\ m^{-3}$, a range that bracketed higher regional-scale anthropogenic pollution[35] (Supplementary Fig. 2b). Taken together, this shows that the aerosol pollution was most pronounced in the hotspot emission regions yet extended over a large area of E. Asia and neighbouring ocean regimes under the prevailing northwesterly winds regime at this time of the year.

Regional carbonaceous aerosols and relationships with sources and processes

Simultaneous measurements of OC, WS-BrC and EC loadings in megacities and surrounding suburban sites were used to examine the regional carbon aerosols for the E. Asia January 2014. The highest levels of OC and WS-BrC were observed in BTH ($49 \pm 21\ \mu g\ m^{-3}$; $14.7 \pm 5.8\ \mu g\ m^{-3}$) and Beijing ($31 \pm 17\ \mu g\ m^{-3}$; $9.8 \pm 5.6\ \mu g\ m^{-3}$) in northern China, followed by SC ($31.6 \pm 11.4\ \mu g\ m^{-3}$; $13.5 \pm 4.4\ \mu g\ m^{-3}$), PRD ($26.4 \pm 11.6\ \mu g\ m^{-3}$; $10.9 \pm 5.0\ \mu g\ m^{-3}$), YRD ($18.2 \pm 10.9\ \mu g\ m^{-3}$; $6.1 \pm 3.4\ \mu g\ m^{-3}$), Shanghai ($6.7 \pm 3.3\ \mu g\ m^{-3}$; $3.1 \pm 1.6\ \mu g\ m^{-3}$) and lowest at KCOG ($3.3 \pm 2.9\ \mu g\ m^{-3}$; $2.2 \pm 2.0\ \mu g\ m^{-3}$) (Fig. 1b–e, Supplementary Table 2). The EC, an indicator of primary aerosol emissions from incomplete combustion, was identically highest concentrations in Beijing/BTH (~$7.5 \pm 3.9\ \mu g\ m^{-3}$) compared to other continental sites (range from 1.6 ± 0.7 to $4.8 \pm 1.8\ \mu g\ m^{-3}$), which in turn was higher than at the regional receptor site KCOG ($0.7 \pm 0.7\ \mu g\ m^{-3}$). The observed OC-to-EC ratios at KCOG (4.7 ± 0.9) were comparable with the inland sites (4 ± 1 to 7.4 ± 2.6), suggesting a roughly regional signature of carbon aerosols.

In E. Asia, the WS-BrC-to-OC ratio versus EC concentration showed that the fraction of WS-BrC/OC was approximately 65% at low levels of incomplete combustion marker EC (e.g., KCOG, see Fig. 2a). Compared to the regional receptor KCOG, EC levels were higher in the source regions, and a decreasing WS-BrC/OC ratio (in turn, an increasing water-insoluble OC (=OC – WS-BrC) to OC ratio from receptor to source) reached an asymptote as EC approached infinity (Fig. 2a, Supplementary Fig. 3a). The variability of EC loadings in the source region (e.g., EC levels spanning from ~3 to $12\ \mu g\ m^{-3}$ for Beijing/BTH) may be due to a shift of meteorology or emission strengths, but the signature for the source area regime—imprinted in the WS-BrC-to-OC ratio—remained constant in the source region (e.g., $31 \pm 3\%$ for Beijing, $31 \pm 5\%$ for BTH; Figs. 1e, 2a). In parallel to E. Asia, we find an analogue trend in S. Asia, as shown in Fig. 2b. This consistent behaviour was further assessed using our theoretical model calculations for the different source regimes, i.e., E. and S. Asia (model details in Supplementary Note 2). The model shows the ability to capture the evolution of WS-BrC/OC vs. EC loadings over both E. and S. Asia (Fig. 2, Supplementary Fig. 3). The overall model function outputs a limit or threshold of ~0.30 for the WS-BrC/OC ratio in the region with high EC concentrations, which may suggest the typical characteristic of fresh atmospheric aerosols in the source regions. This threshold alines with our mean observational values in the high-emission source areas.

In the polluted winter, the low ratio (~0.30) of WS-BrC/OC in the source regions of E. and S. Asia may imply that OC has not yet had enough time to oxidize fully into WS-BrC. In contrast, the high/increasing WS-BrC/OC ratios under its corresponding EC concentrations indicate certain OC was oxidized to WS-BrC as aerosols became diluted (due to sinks or dispersion) during air mass transport. The high WS-BrC/OC ratios under its corresponding loadings of EC reflect the evolution/oxidation of aged OA and transported particles. The higher the ratios are (>0.4; typically with low EC concentrations), the farther the aerosols may be transported and/or the more aged they are, thus another complementary method (WS-BrC/OC vs. EC) to diagnose the oxidation state of OA, for instance, O:C ratios were used as a metric of the oxidation state of OA[50]. Our introduced source-to-evolution concept for WS-BrC/OC vs. EC distinguishes fresh and aged carbon aerosols. It predicts the trend of carbon aerosol subcomponents during OA's oxidative evolution and transport.

Taken together, the WS-BrC/OC vs. EC model successfully simulated both E. Asia and S. Asia and compared well with the

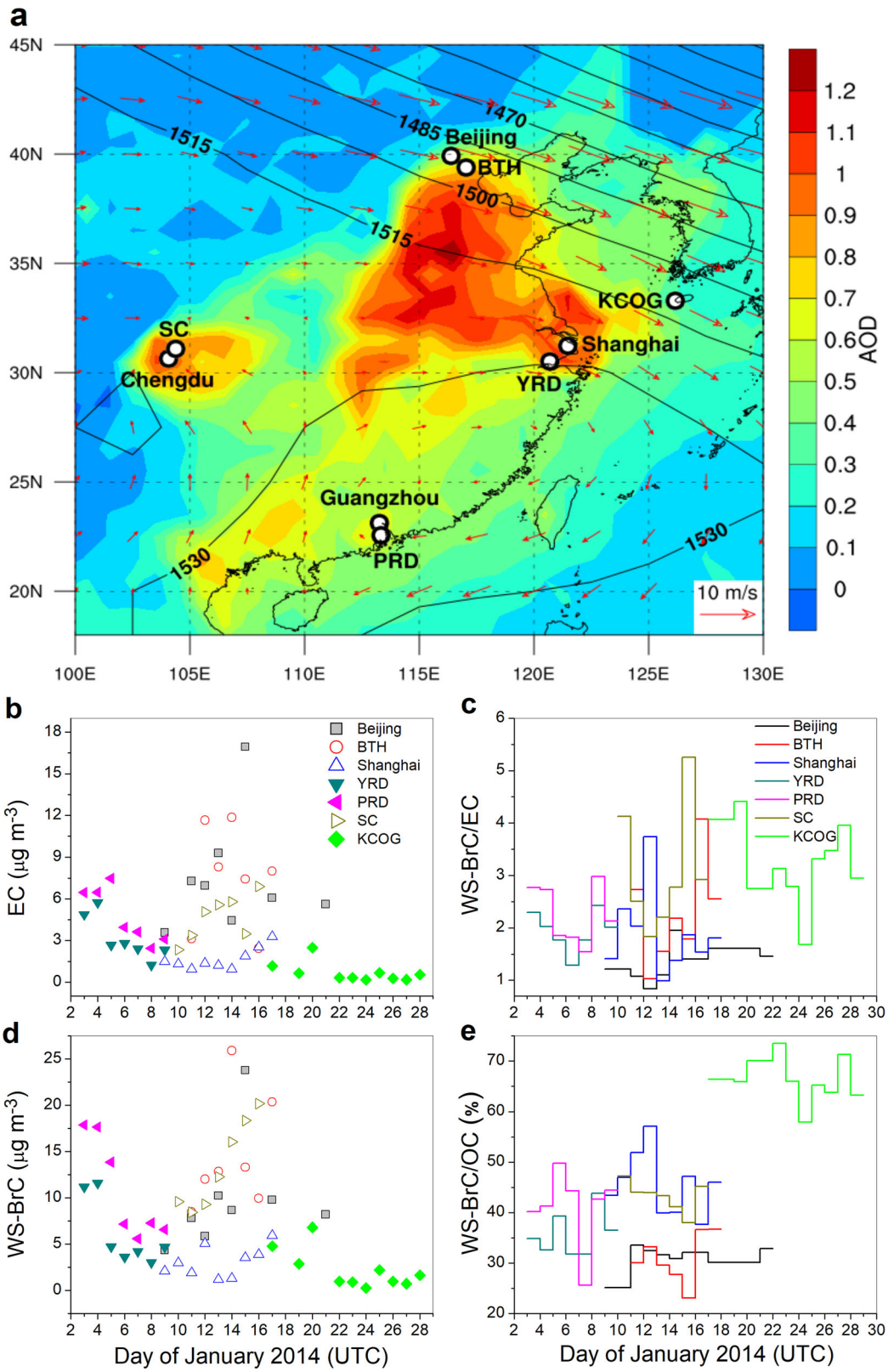

observations. For source-to-receptor transported aerosols in E. and S. Asia, the results suggest the oxidation/air transport processes could dynamically increase WS-BrC-to-OC ratios during the dispersal/transport of primary incomplete combustion emissions (recalcitrant EC).

Linking light-absorption properties of WS-BrC to source regimes

This section discusses the relationship between two optical properties (MAC and AÅE; 'Methods') and anthropogenic pollution sources. The MAC serves as a proxy of aerosol radiative forcing

Fig. 1 AOD and temporal variability of carbonaceous aerosols in East Asia during January 2014. a AOD map and synoptic weather pattern in Jan-2014. The black and white circles denote the locations of the sampling sites, including urban sites Beijing and Shanghai, and inland regional sites BTH (Tianjin in the Beijing-Tianjin-Hebei region, China), YRD (Haining in the Yangtze River Delta, China), PRD (Zhongshan in the Pearl River Delta, China), SC (Deyang in Sichuan province, China) and SE Yellow Sea receptor KCOG (Korea Climate Observatory at Gosan, Jeju Island). **b**, **d** The concentrations of EC and WS-BrC. **c**, **e** The ratios of WS-BrC-to-EC and WS-BrC-to-OC. The same colour is employed for the same site. The symbols denote the concentrations, while the coloured horizontal step lines show the ratios. Concentration and ratios in Beijing, BTH, Shanghai and KCOG are from ref. [35]. The monthly average AOD data at 550 nm were obtained from NASA Moderate Resolution Imaging Spectroradiometer (MODIS) level 3 collection 6. Monthly mean NCEP/NCAR reanalysis wind vectors (m s^{-1}) and geopotential height at 850 hPa pressure level were used to illustrate regional-scale circulation.

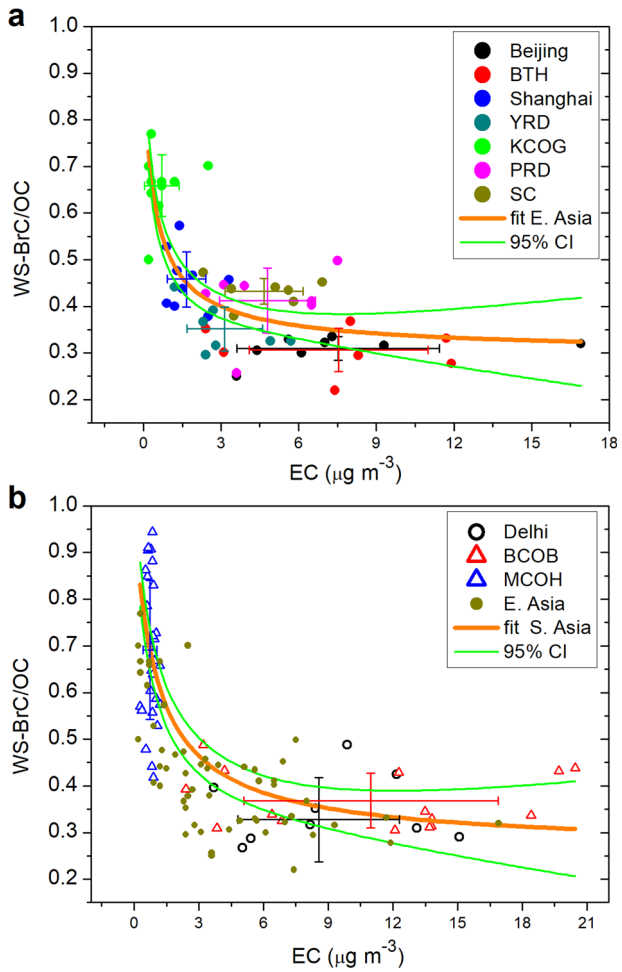

Fig. 2 A conceptual model for WS-BrC/OC vs. EC during aerosol transport. Relationship between WS-BrC-to-OC ratios and EC concentrations in $PM_{2.5}$ over East Asia (**a**) and South Asia (**b**): inter-site comparison over E. and S. Asia as well as the convergence of overall trends from the continental emission source areas to the ocean background receptor sites. A conceptual model function (equation (11) in Supplementary Note 2) is fitted to WS-BrC-to-OC ratios vs. EC loadings, with asymptotic C/D values being 0.30 for E. Asia ($k = 0.83$; root-mean-square deviation (RMSD) of 0.09) and 0.28 for S. Asia ($k = 0.92$; RMSD of 0.15). These asymptotic C/D values indicate their typical characteristics of fresh aerosol in the corresponding emission source regions. **a** All data measured from simultaneously collected $PM_{2.5}$ samples in January 2014. **b** Concentration data for winter S. Asia (e.g., urban Delhi: central Indo-Gangetic Plain (IGP); IGP outflow site BCOB: Bangladesh Climate Observatory at Bhola; Indian Ocean regional receptor MCOH: Maldives Climate Observatory at Hanimaadhoo) in 2016 from earlier study[39]. Error bars in panels (**a**) and (**b**) denote the average values with s.d. for each site.

and the aerosol mass represented in models. The wavelength dependency of the absorbance of WS-BrC is given as Absorption Ångström Exponent (AÅE)[51]. The relative contributions of fossil versus biomass (f_{bio}; $f_{fossil} = 1 - f_{bio}$) to the atmospheric carbonaceous aerosols (e.g., WS-BrC and EC) in the current E. Asia and other S. Asia campaigns[35,37,40,43,47,48,52,53] were quantitatively calculated based on equation (1), as shown in Fig. 3 (for details about calculation, see 'Source apportionment' in Methods; for source endmembers, see Supplementary Table 3; for raw isotope data, see Supplementary Table 4; for source apportionment results, see Supplementary Table 5). Unlike concentration and molecular markers, radiocarbon isotopic fingerprinting is intrinsic, and isotope ratios are intensive properties that are more stable than extensive properties such as concentration-based data. The geographically conservative nature of isotopes showed little variability in the sources in both E. and S. Asia (details discussed in 'Methods'). The observed f_{bio} of WS-BrC was ~20–30% higher than that of EC, consistent with BB yielding more water-soluble carbon than vehicle emissions[12,19,54].

In the current absorption measurements during January-2014 East Asian haze, Fig. 4 showed that the optical signatures of two more-coal-affected sites (i.e., Beijing/BTH) were well outside the trend of other less-coal-affected sites and distributed in the upper right corner. This coal-impacted WS-BrC, a mixture strongly influenced by high coal-burning emissions together with other source contributions (e.g., BB and liquid fossil), was characterized by higher AÅE (~5–9.3) under the same corresponding MAC in the real atmosphere. We note that the observed MAC and AÅE for ambient WS-BrC reflected a mixture contribution from different sources (e.g., BB, coal and liquid fossil), while likely with a different proportion (i.e., MAC and AÅE of respective sources multiply fraction sources). A higher AÅE means the absorption weighs more toward shorter wavelengths. Previous laboratory source tests suggest that coal-burning yields light-absorbing WS-BrC[16,17,46,55]; some of the previously reported MAC and AÅE values for source emission tests and ambient measurements are available in Supplementary Table 6. These laboratory coal-fire measurements of WS-BrC MAC_{365nm} reported a large range of values, depending on the fuel and burning conditions and measurement protocol. The recently reported MAC_{365nm} for coal burning (e.g., 1.3 ± 0.34 m^2 g^{-1}, 2.0 ± 0.75 m^2 g^{-1}, 1.1 ± 0.16 m^2 g^{-1})[17,46] is comparable with the strong light absorption of BB-produced WS-BrC (e.g., 1.6 ± 0.6 m^2 g^{-1} (ref. [17]); 0.79–1.56 m^2 g^{-1} (ref. [56]); 1.0 ± 0.3 m^2 g^{-1} (ref. [42])). However, the previous laboratory source tests showed a clear trend of $AÅE_{330-400nm}$ between coal and BB; coal AÅEs on average (e.g., 11–13 (ref. [55]); 9.6 ± 1.8 (ref. [46])) were much higher (towards to right-hand on the x-axis of AÅE) than biomass-burning AÅEs (6.7–8.6 (ref. [55]); ~7 for $AÅE_{330-400nm}$ of methanol-soluble OC from ref. [57]). At the same MAC, the observed higher AÅE in Beijing/BTH, relative to other less-coal-impacted sites, is in line with the general trend of AÅE found in previous laboratory source-fire tests (coal has higher AÅE than BB). Since other sources (e.g., BB) bearing lower AÅE (relative to coal fuel-burning) also contributed to Beijing/BTH WS-BrC, the lower AÅE sources could reduce AÅE in

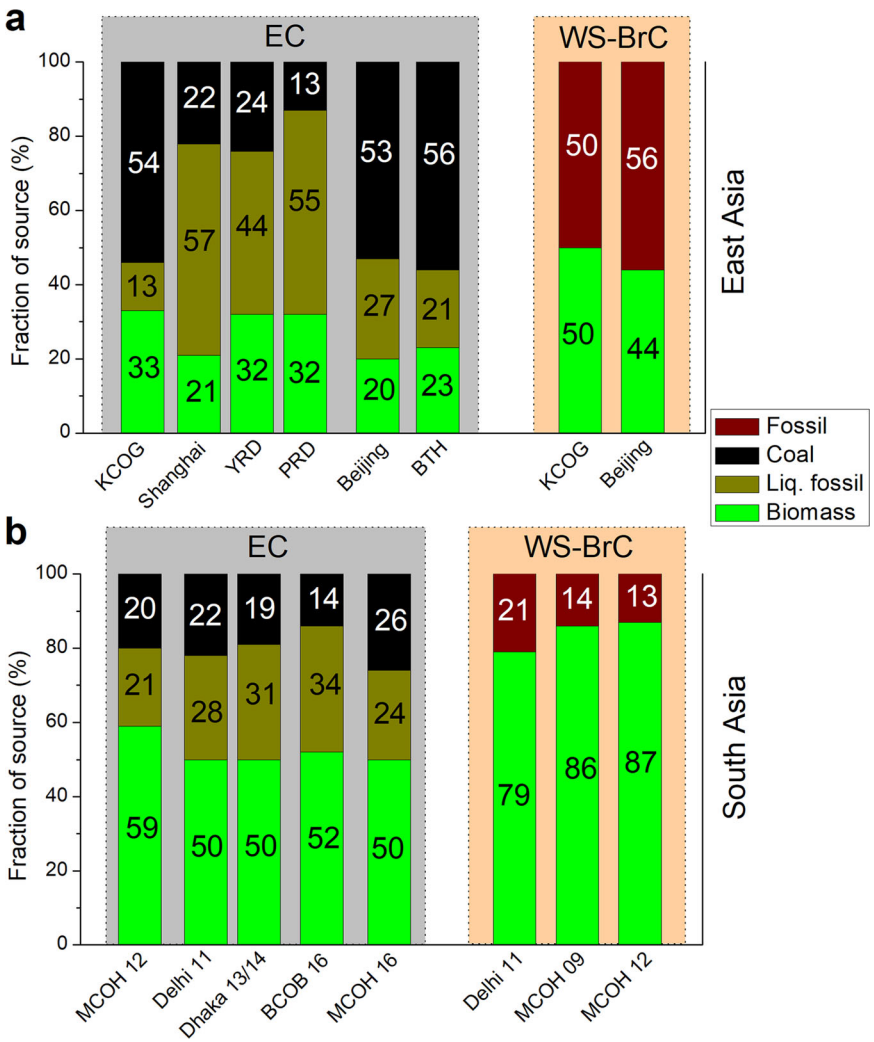

Fig. 3 The source contribution of respective EC and WS-BrC in $PM_{2.5}$ over East Asia and South Asia. The dual-carbon ($\Delta^{14}C$ and $\delta^{13}C$) isotope-based source apportionment of respective EC and WS-BrC in $PM_{2.5}$ over East Asia (**a**) and South Asia (**b**): inter-site comparison over E. and S. Asia as well as the comparison between the continental emission source areas and the ocean background receptor sites. The stack columns depict the fraction sources to EC (grey shaded) and WS-BrC (brown shaded). Suffix numbers on the x-axis of panel (**b**) define the campaign year, e.g., MCOH 12 means MCOH 2012. Here the fractions of sources were computed by MCMC technique with the same endmembers of sources. Raw isotope data for E. Asia: Shanghai, Beijing, BTH and KCOG in winter (January) 2014 from Fang et al.[35], winter (January) 2013 in YRD and PRD from Fang et al.[47]; S. Asia: winter 2012 MCOH from Bosch et al.[37], winter 2013/14 Dhaka from ref. [52], winter 2016 in both BCOB and MCOH from ref. [53], winter 2009 MCOH from ref. [43], while Delhi_WS-BrC and Delhi_EC isotope in winter 2011 from Kirillova et al.[40] and Bikkina et al.[48], respectively.

the mixture of Beijing/BTH ambient samples. As a result, the observed AÅE (Beijing/BTH) is more likely lower than the values measured in previous single-coal-fuel burning tests. In addition, atmospheric ageing may also impact the optical properties of WS-BrC. A recent coal-burning chamber study indicated that OH-initiated ageing could reduce both MAC and AÅE of BrC[16]. However, the effects could be much different in the real ambient regime due to extremely high concentrations of emission and oxidants as well as limited duration in the smog chamber[7,11–15,21,22]. The varying burning conditions and fuel types, aerosol complexity, evolution and lifetime for ambient aerosols could cause the laboratory test results to differ from ambient measurements[11–21]. Taken together, the available reported laboratory source tests support our discovery of distinctly high AÅEs at corresponding MACs for coal-influenced WS-BrC in the real atmospheric haze.

Not all WS-BrC substances absorb light to the same extent at the studied wavelengths, which in turn impacts the total MAC. For MAC_{365nm} versus AÅE in E. and S. Asia, a comparison of the results shows a qualitatively similar trend for the two regions, but the 'slope' is much sharper in S. Asia (Fig. 5a). The MAC_{365nm} follows an exponential decay function against AÅE for only the similar source regime (e.g., E. Asian sites with similar fraction sources such as Shanghai, YRD, PRD and SC; all S. Asian sites with similar source shares), while the inherent physical meaning for this empirical equation is currently unclear. Except for Beijing/BTH source region in E. Asia, the coal played a much lower role in both S. Asia and other E. Asia sites (for source shares, see Fig. 3). The similar coal contribution in S. Asia and E. Asia (less-coal sites) eases the comparison of MAC contributed by the other two main sources (biomass burning and liquid fossil). The fractional contribution of biomass to WS-BrC in S. Asia was ~80%, whereas it was ~50% in E. Asia (Fig. 3 and Supplementary Table 4; refs. therein). The BB was expected to be the dominant contribution of biomass/biogenic sources of OC and WS-BrC during the high anthropogenic emission-generated winter pollution episodes[35,40,43]. Furthermore, the fraction of liquid fossil ($f_{liq\ fossil}$) to EC in E. Asia, except for Beijing/BTH, is generally ~20 to 30% higher than that in S. Asia.

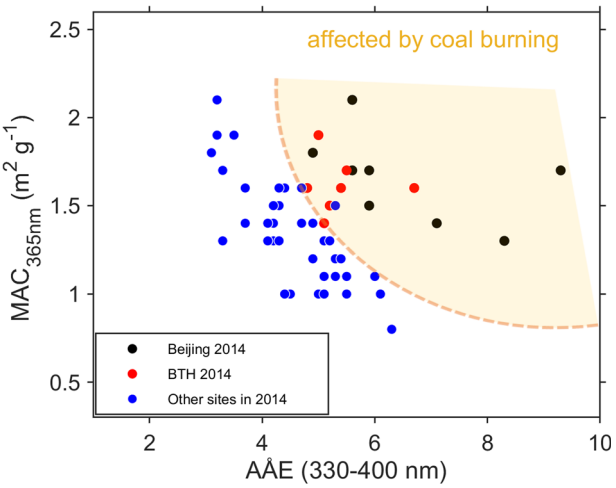

Fig. 4 Contrasting solar-absorption parameters of WS-BrC in sites affected by expected higher coal-combustion emission compared to other sites with lower coal-burning emission. The relative source contributions to EC for representative Jan-2014 samples in Beijing, BTH and Shanghai are shown in Fig. 3. For measured MAC_{365nm} versus AÅE during January 2014 E. Asian haze, the optical signatures of high coal-combustion impacted samples (gold shaded) are well outside the trend of other sites, implying a strong influence of coal combustion source (for MAC and AÅE calculations, see 'Measurement of the optical properties of WS-BrC' in Methods). The observed ambient MAC and AÅE reflected a mixture contribution from different sources (e.g., biomass burning, coal and liquid fossil). The BTH denotes the rural sampling site at Tianjin, a representative atmosphere of the Beijing-Tianjin-Hebei region.

Comparing the $MAC_{WS\text{-}BrC}$ of E. Asia (Shanghai, YRD, PRD and SC) to that of S. Asia (Delhi and BCOB), Fig. 5a shows that the light absorption of BB-dominated (f_{bio}, ~80%) S. Asian WS-BrC is stronger than that of vehicle-affected (f_{fossil}, ~50%) E. Asian WS-BrC in the near emission source sites. Furthermore, our observed $MAC_{WS\text{-}BrC}$ at the KCOG receptor site as a function of radiocarbon signature during the Jan. 2014 pollution period also reveals that increasing modern carbon (f_{bio}) in WS-BrC increases MAC_{365nm} (Supplementary Fig. 4). This may indicate that the MAC will be strongly diluted if vehicle emission provides WS-BrC of low MAC. In winter Switzerland, fresh BB smoke was found to have the highest MAC (1.4 $m^2\ g^{-1}$), followed by oxygenated OC (aged OA; 0.7 $m^2\ g^{-1}$), and only 0.13 $m^2\ g^{-1}$ for the other less absorbing OC[58]. In another developed region, N. America, much lower WS-BrC MAC_{365nm} was found in urban ambient (e.g., Atlanta, Georgia, Los Angeles), where the fossil emissions (e.g., vehicle) were expected to be high[45,59,60]. For the laboratory source tests, the previously reported MAC_{365nm} for collected samples near a diesel motorcycle was much lower (e.g., 0.2 $m^2\ g^{-1}$ from ref. [42]; 0.26 $m^2\ g^{-1}$ for methanol-SOC from ref. [17]) than other near-source and BB samples. Based on wavelength dependence investigation by a filter-optical-transmission method, Kirchstetter et al. suggested that on-road vehicle emission aerosols produce much less absorbing BrC than BB[22]. Thus, the source measurements are in line with our findings regarding the source contributions of water-soluble BrC in the atmospheres of E. and S. Asia.

A Monte Carlo simulation (MC; for MC simulation details, see Supplementary Note 3), with a random sampling of our observational parameters of MAC_{365nm} (including Shanghai, YRD, PRD and SC from E. Asia, and Delhi as well as BCOB from S. Asia) and fraction sources of BB and fossil fuel, yields an interquartile range (IQR) of MAC_{365nm} for the respective sources. The probability density distributions (PDD) of source-resolved $MAC_{BB\text{-}predicted}$ for BB and $MAC_{fossil\text{-}predicted}$ are shown in Fig. 5b, c. A considerably lower median of $MAC_{fossil\text{-}predicted}$ (median: 1.15 $m^2\ g^{-1}$; highest PDD: 0.80 $m^2\ g^{-1}$) than that of $MAC_{BB\text{-}predicted}$ (median: 1.72 $m^2\ g^{-1}$; highest PDD: 1.86 $m^2\ g^{-1}$) indicates the fossil-fuel WS-BrC in more vehicle emission-affected areas in E. Asia was presumably less absorbing than BB WS-BrC at the studied wavelengths. Thus, the source measurements and model simulations align with our findings regarding the source contributions of water-soluble BrC in the atmospheres of E. and S. Asia.

The relationship between bleaching and isotope effects during air transport

During aerosol transport, atmospheric processing through photochemical oxidation would be expected to simultaneously influence the light absorption and stable carbon isotope composition of WS-BrC. Besides the source-diagnostic ability, the stable carbon isotope $\delta^{13}C$ provides important information on atmospheric processing for WS-BrC aerosol samples[35–37,39,43]. In the current study period in E. Asia, Back Trajectories (BTs) analysis (Supplementary Figs. 5 and 6) showed that the KCOG samples intercepted the prevailing outflows from BTH and northern China. Here we observed for East Asia that WS-BrC MAC_s were decreasing from Beijing to KCOG, with $\delta^{13}C_{WS\text{-}BrC}$ signatures concurrently becoming enriched (more positive) along with the air mass transport (Fig. 6). The relatively lower MAC_{365nm} at KCOG compared to Beijing/BTH reflected atmospheric bleaching of WS-BrC during this long-range transport. These changes in MAC and $\delta^{13}C$ were likely not from entrainment and mixing with other WS-BrC during the transport trajectory because, in addition to the BTs, the radiocarbon $\Delta^{14}C_{WS\text{-}BrC}$ and $\Delta^{14}C_{EC}$ data of synoptic samples showed similar source shares between source area (f_{bio} of WS-BrC: 44 ± 4%) and the Yellow Sea regional receptor site KCOG (f_{bio} of WS-BrC: 50 ± 8%) (Fig. 3a). Some minor local entrainments at KCOG cannot be completely ruled out, this is likely insignificant and will not substantially affect the light absorption and $\delta^{13}C$ of the WS-BrC. This similarity in radiocarbon signal is consistent with the fact that the WS-BrC in the continental source region is also dominating the WS-BrC at the background receptor site. Furthermore, the location of the KCOG was carefully selected in a remote region of Gosan Island, on an ocean cliff on the side of the island receiving the outflow from continental East Asia. This revelation of a strong bleaching effect for WS-BrC in E. Asia is consistent with the patterns recently deduced in a study from S. Asia, where a much lower WS-BrC MAC_{365nm} (0.4–0.5 $m^2\ g^{-1}$ from ref. [37]) was observed at the Indian Ocean receptor site Maldives Climate Observation at Hanimaadhoo (MCOH) compared to source regions (e.g., Delhi; 2.5 ± 0.3 $m^2\ g^{-1}$ from ref. [39]), despite a higher BB contribution in S. Asia.

Our E. and S. Asian and other field studies have suggested that photochemical ageing (e.g., photooxidation, photo-dissociation) during transport can oxidize the organic matter with the remaining WS-BrC $\delta^{13}C$ signature becoming increasingly enriched[35,37,39,43,61,62]; for instance, ageing induces a fractionation in the aerosol $\delta^{13}C$, leading to an increasing $\delta^{13}C$ signal in the remaining aerosols, consistent with kinetic isotope effects (KIE) induced preferential fragment/removal of lighter carbon isotopes (^{12}C) in small functional groups[35,37,43,61,62]. On the other hand, some chamber studies have shown that the $\delta^{13}C$ KIE during gaseous hydrocarbons to particle SOA formation induces SOA products to be isotopically depleted, which may be due to VOCs carrying isotopically lighter carbon reacting faster to form SOA products with lighter carbon[63,64]. It should be noted that SOA formed from the oxidation of gas hydrocarbons differs from the photochemical ageing of aerosol particles. Strictly speaking, SOA material is formed in the atmosphere by the mass transfer to the aerosol phase of low vapour pressure products of the oxidation of organic gases, requiring both a gas phase chemical transformation and a change of phase[4,65–69]. The previous laboratory-observed

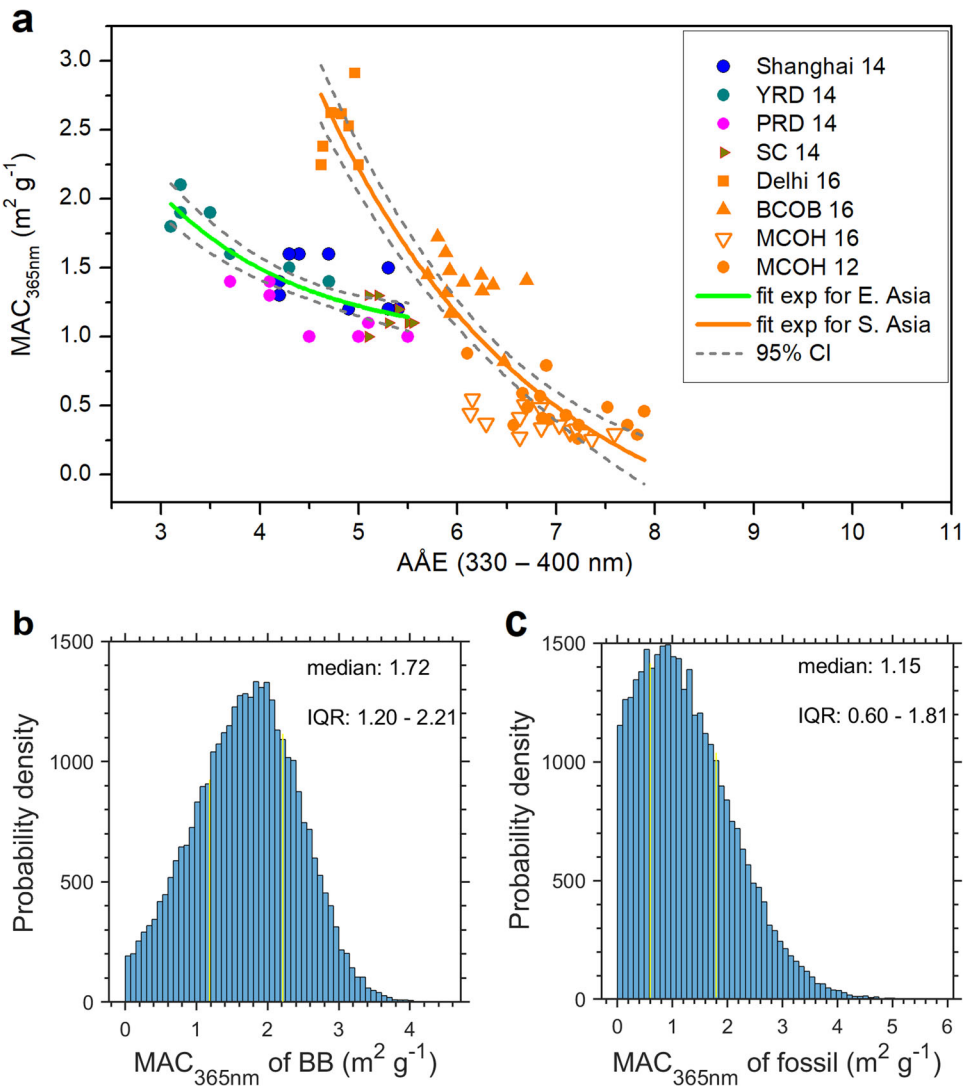

Fig. 5 The link of light-absorption properties of WS-BrC to source regimes. a A comparison of the trend of WS-BrC MAC_{365nm} vs. AÅE between current 2014 E. Asian study (less-coal areas) and earlier S. Asian studies (less-coal areas, data integrated for winter 2016 Delhi, BCOB, MCOH from ref. [39], winter 2012 MCOH[37]). Green line shows the exponential fit for E. Asia, while the orange line represents the exponential fit for S. Asia. The grey dashed lines are the 95% confidential intervals for the fittings. Suffix numbers show the campaign year, e.g., 16 denotes 2016. Probability distributions of source-resolved MAC_{365nm} for $MAC_{BB\text{-}predicted}$ (**b**) and $MAC_{fossil\text{-}predicted}$ (**c**). The distributions are derived from the Monte Carlo simulation (for MC simulation details, see Supplementary Note 3), using our observational data of MAC_{365nm} (including Shanghai, YRD, PRD and SC from E. Asia, and Delhi and BCOB from S. Asia) and relative source contributions (i.e., Fig. 3). Medians and interquartile range (IQR) of MAC_{365nm} are given for respective sources. Yellow lines mark the IQR.

$\delta^{13}C$ isotope effects during gas hydrocarbons to particle SOA indeed may induce total SOA products to be either isotopically depleted (negative) or so small and indistinguishable shift of $\delta^{13}C$ from its precursor[63,64,68,69]. However, our observed $\delta^{13}C_{WS\text{-}BrC}$ during source-to-receptor transport was largely enriched (positive), opposite to $\delta^{13}C$ isotope effects on SOA. In wildfire plumes, previous measurements showed little to no net change in BB-OA[15,29–31], and BrC absorption decayed after emission[15,32]. Another recent field BB-plumes study[23] suggested that, after the initial 3–6 h daytime oxidation, SOA from the primary gas precursors contributes only ~4% of total OA mass, with the other SOA from oxidation of evaporated primary OA (particle-gas-particle processes) accounting for ~30% of total OA mass and primary OA comprising the rest (~66%). In a sense, SOA formed from the oxidation of evaporated primary OA is very similar to the photochemical ageing of primary OA due to the same sources and chemical structures of primary OA. Using a limiting case test for SOA, a two-fold reduction of $MAC_{WS\text{-}BrC}$ at KCOG may not be from SOA formation (test detailed in 'Methods'). One possible explanation is that there must be large atmospheric bleaching of WS-BrC during long-range oversea transport.

In addition, OC-to-EC ratios, another rough but highly uncertain indicator of sources, primary emissions and secondary processes, were expected to have much higher ratios in secondary relative to primary for the same or similar emission sources[4,13,19,20]. However, our observed ratios were approximately constant at the ocean background site KCOG (4.7 ± 0.9) compared with the inland sites (e.g., Beijing: 4.3 ± 1.2; Shanghai: 4.0 ± 1.0). Combined with constant $\Delta^{14}C_{WS\text{-}BrC}$ and $\delta^{13}C_{WS\text{-}BrC}$ shifts between continental sites and the KCOG, it implies that SOA formation from primary gas precursors during oversea transport may not be a significant contributor. Taken together, our observed decreasing MAC and increasing $\delta^{13}C_{WS\text{-}BrC}$ at the ocean background site after long-range transport from the source region suggests that photochemical ageing (i.e., a particle-to-aged particle process) would likely play an important role in this aged WS-BrC pool rather than

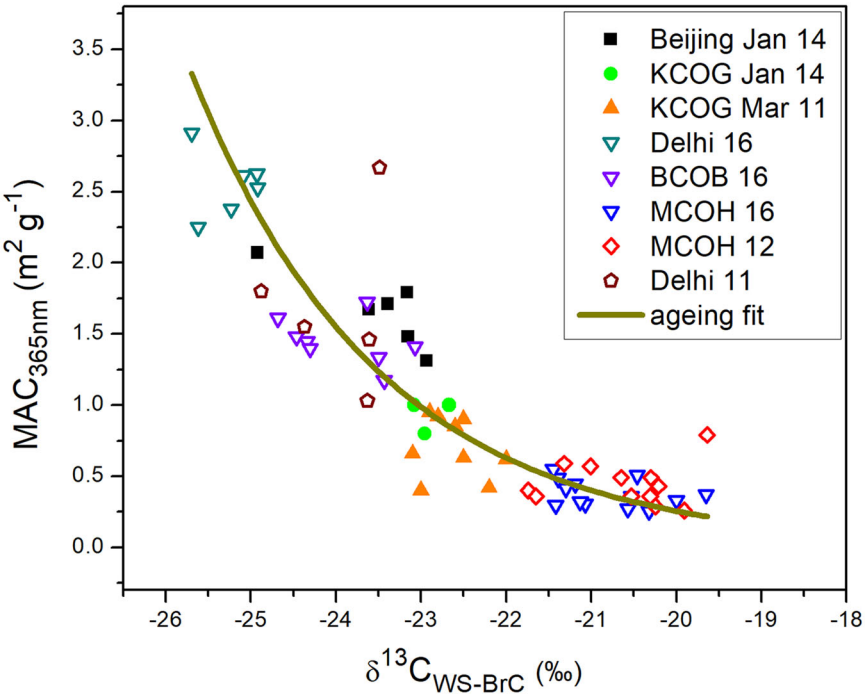

Fig. 6 Atmospheric bleaching of mass absorption cross-section against stable isotope composition of WS-BrC consistent with ageing during source-to-receptor transport in Asia. Scatter symbol depicts measurements of optical parameter MAC_{365nm} and the corresponding stable carbon isotope ratio for WS-BrC from the current 2014 E. Asian campaign, earlier KCOG pollution events (KCOG 11)[36] and S. Asian campaigns (MCOH 12)[37], (Delhi 16, BCOB 16, MCOH 16)[39], (Delhi 11)[40]. Suffix numbers show the campaign year, e.g., 14 denotes 2014. A first-order kinetic model fit (dark yellow line) reveals the interdependence of MAC_{365nm}, $\delta^{13}C_{WS\text{-}BrC}$ and atmospheric processing (i.e., the bleaching effect from photochemical/oxidation ageing); $\delta^{13}C_{WS\text{-}BrC}$ is used as a proxy for ageing, see Supplementary Note 4 for model fit during aerosol transport in the Asian outflows. The goodness for the best-fit curve is with the RMSD of 0.34.

SOA formation from primary VOCs oxidation. Indeed, a growing body of evidence from laboratory studies also suggests photolysis and oxidation of the conjugated structures of chromophores and photochemical ageing of BrC may reduce its light absorption[7,14,16,21,58,70–74]. Numerous ageing processes are expected to proceed for OC aerosols during the day-to-week time scales before they undergo wet or dry deposition from the atmosphere. One of the leading conclusions from the previous investigations is that significant photobleaching and oxidative whitening will occur when BrC is a day or more distant from its source (ref. [74], and refs. therein). Direct photolysis of BrC (or OC) molecule and indirect photo-initiated (sunlight produces OH, $^1O_2$) oxidation can occur either in the aerosol particles or when they are incorporated into cloud droplets. For example, a previous BB BrC study showed that the absorption decreased continuously with UV light exposure[75]. Another chamber study indicated a significant fraction of the apparent decreases of BrC in aged BB plumes through the continued oxidation of nitrophenols (important light-absorbing compounds in BB emissions) into products with fewer or weaker chromophores[23]. This reduced absorption due to UV light exposure indicates the relative importance of photolysis, or breakdown of chromophores, compared to SOA formation. Other laboratory simulation studies on aqueous OH oxidation of individual nitrophenol suggested that the absorption loss may link to the formation of fragmented products from cleavage of the aromatic ring with continued OH oxidation[76,77]. Heterogeneous oxidation can also occur, in which a gas-phase oxidant (such as OH, NO_3 or O_3) collides with an aerosol particle, resulting in changes in chemical and thus $\delta^{13}C$ and light absorptivity of WS-BrC[74].

The degradation of WS-BrC by ambient photolysis and oxidation can be estimated to be a pseudo-first-order reaction[39] (for kinetic model details, see Supplementary Note 4). To test this bleaching effect for both S. Asia and E. Asia, we examined the relationship between the time evolution of $MAC_{WS\text{-}BrC}$ and stable carbon isotope signature $\delta^{13}C_{WS\text{-}BrC}$ during long-range oversea transport from source to a receptor in both regions using bleaching equation (28) in Supplementary Note 4. A high interdependency of $MAC_{WS\text{-}BrC}$ vs. the ageing proxy $\delta^{13}C_{WS\text{-}BrC}$ is found for the combined East and South Asia data (Fig. 6). This dynamic bleaching pattern of water-soluble BrC is thus holding for both E. and S. Asia, even though the dominant sources in the regions were quite different. This supports the hypothesis that the atmospheric photolysis/oxidation processes destruct chromophores from any sources to reduce WS-BrC absorptivity during the transport of anthropogenic aerosol pollution (a summary illustration of these processes expected to affect the isotope and light-absorption can be found in Supplementary Fig. 7).

For quantitatively estimating the bleaching effect in E. Asia, the bleaching rate k (day^{-1}) for the WS-BrC during source-to-receptor dispersion was calculated using the first-order empirical decay Eq. (6) (see 'Methods'). Average air mass transport times were estimated based on the BTs analysis (Table 1). The observed bleaching rate k ranged between 0.13–0.35 day^{-1} with a mean value of 0.24 ± 0.10 day^{-1} (Table 1, Supplementary Fig. 8). This rate is comparable to the findings for S. Asia, where k was 0.20 ± 0.05 day^{-1}. This bleaching of water-soluble BrC corresponds to an atmospheric half-life of 2.9 ± 1.0 days and reduces $MAC_{WS\text{-}BrC}$ ~ 50% during the initial 3 days by atmospheric ageing for the E. Asian outflow. The consistency of BrC bleaching parameters independently found in E. and S. Asian outflows indicates that the weakening of the light-absorption of BrC is a prevalent phenomenon, which is probably related to the photochemical process rather than the sources of light-absorbing BrC.

Table 1. First-order bleaching rate k (day^{-1}) for WS-BrC during the dispersal of E. Asian haze.

Site-sample ID	$MAC_{KCOG\text{-}WS\text{-}BrC}$ ($m^2\ g^{-1}$)	$MAC_{Beijing\text{-}WS\text{-}BrC}$ ($m^2\ g^{-1}$)[a]	Air transport time estimate (t, hour)[b]	Bleaching rate (k, day^{-1})[c]	Bleaching percentage (%)	Air masses passed over source region
KCOG-0117	0.8 ± 0.05	1.7 ± 0.2	88 ± 14	0.21 ± 0.07	53 ± 8	Beijing/BTH
KCOG-0119	1.0 ± 0.05		66 ± 2	0.19 ± 0.05	41 ± 6	Beijing/BTH
KCOG-0120	1.0 ± 0.02		41 ± 25	0.31 ± 0.25	41 ± 8	Beijing/BTH
KCOG-0122	1.3 ± 0.05		44 ± 2	0.15 ± 0.05	24 ± 10	Beijing/BTH
KCOG-0123	1.3 ± 0.03		48 ± 7	0.13 ± 0.05	24 ± 11	Beijing/BTH
KCOG-1	0.85 ± 0.05		58 ± 6	0.28 ± 0.09	50 ± 8	Beijing/BTH
KCOG-5	0.92 ± 0.06		60 ± 4	0.25 ± 0.09	46 ± 13	Beijing/BTH
KCOG-6	0.90 ± 0.05		71 ± 12	0.21 ± 0.10	47 ± 10	Beijing/BTH
KCOG-7	0.95 ± 0.06		72 ± 6	0.19 ± 0.08	44 ± 9	Beijing/BTH
KCOG-9	0.40 ± 0.05		98 ± 12	0.35 ± 0.12	76 ± 6	BTH/Yellow sea
KCOG-10	0.42 ± 0.0.5		100 ± 15	0.33 ± 0.06	75 ± 6	BTH/Yellow sea
Mean	0.89 ± 0.28		68 ± 19	0.24 ± 0.10	47 ± 18	

[a]Mean $MAC_{Beijing\text{-}WS\text{-}BrC}$ (365 nm) measured in this study was used for the bleaching rate constant calculation. (The KCOG-1 to -10 samples and data of $MAC_{KCOG\text{-}WS\text{-}BrC}$ are from ref. [36]).
[b]Air transport time from source region (e.g., Beijing) to KCOG receptor was on average estimated based on NOAA HYSPLIT BTs for the corresponding sample, shown with mean and standard deviation.
[c]k values were calculated by the presumed Eq. (6).
The KCOG and BTH refer to the Korea Climate Observatory at Gosan and the Beijing-Tianjin-Hebei region of China, respectively.

Comparison of the relative solar absorption by WS-BrC and BC

The fraction (f) solar energy absorbed by WS-BrC relative to BC showed strong wavelength dependency and large variability (from 3 ± 1.0% to 21 ± 9%) between source areas and regional receptors (details on the comparison of total direct absorbance by WS-BrC to BC, see 'Methods'). The f ratios in the current E. Asian study were generally in the range of previous findings in E. Asia[36,41] and S. Asian sources[40]. However, the observed highest values at KCOG (11–21%) were much higher than the mere 0.7 ± 0.2% at the Indian Ocean receptor site MCOH[37]. The larger loss of light absorptivity of WS-BrC at MCOH compared to KCOG was probably due to a transport distance of thousands of kilometres to MCOH (up to one-week transport time) and stronger sunlight (may enhance the reactivity of photolysis and photo-initiated reaction) in the lower latitude of the Indian Ocean. Therefore, it is critical to consider not only the bleaching effects of $MAC_{WS\text{-}BrC}$ but also the changing ratios of these two pools of carbonaceous aerosols during transport.

DISCUSSION

Several factors impact the light absorption of high-loading WS-BrC. Earlier measurements[12–18,20,23,25–32,36–46], only specifically performed for similar source emission regimes or source-burning tests, were challenged to constrain these combined influences of sources and atmospheric ageing on the light absorption properties of BrC, thereby hindering advanced comprehension and modelling of the overall aerosol–climate effects of BrC. The continental source regions and ocean receptors over East Asia and South Asia used as natural laboratories in this study, provide contrasting source regimes and different source-to-receptor transport in revealing the effects on the optical properties of WS-BrC. Our observations showed that coal-impacted WS-BrC has a distinctly high AÅE under the same MAC in the ambient atmosphere of northern China. This phenomenon may be useful in identifying whether aerosol pollution originates primarily from coal combustion or not. Signals of modern ^{14}C indicate a strong inverse correlation between WS-BrC light absorption and age of the source material in both East and South Asia. That is, BB produces higher $MAC_{WS\text{-}BrC}$ than liquid fossil does. Our Monte Carlo simulations further show that low-temperature incomplete BB produces strong light-absorbing WS-BrC. In contrast, high-temperature liquid fossil-fuel combustion, such as a vehicle, produces less-absorbing WS-BrC, thus diluting the overall absorbance of total BrC in the region. If the model improperly uses the light absorption value of BB (or light absorption of fossil) to other fossil fuel-burning dominated (or BB-dominated) regions, it will lead to an overestimation (or underestimation) of WS-BrC absorption, resulting in errors in the radiative forcing assessment. In future modelling efforts, models should adopt different treatments for BB and fossil-fuel-impacted emission regions to reflect their large difference in WS-BrC light absorption.

The enrichment of $\delta^{13}C_{WS\text{-}BrC}$ during long-range oversea transport from the source area to regional receptor suggests photochemical oxidations play important roles in the dynamically changing WS-BrC, rather than additions of SOA from oxidation of VOCs. The strong interdependency of $MAC_{WS\text{-}BrC}$ and ageing proxy $\delta^{13}C_{WS\text{-}BrC}$, while $\Delta^{14}C_{WS\text{-}BrC}$ stays rather invariant, over both East Asia and South Asia supports the hypothesis that atmospheric photolysis/oxidation processes destruct chromophores to reduce WS-BrC absorptivity during aerosol pollutant transport, in turn suggesting the loss of light absorptivity of WS-BrC is a prevalent phenomenon and largely independent of sources.

This study finds that the optical properties of WS-BrC may be parameterized by several relatively simple relationships for both East and South Asia: (i) a common trend of WS-BrC/OC ratio vs. EC level (which reflects the evolution/oxidation state of OA) is successfully simulated by our conceptual model, (ii) a source-dependency of optical characteristics found in Asian atmospheres provides a method to simplify BrC optical parameters, which may be useful in aerosol–climate models, and (iii) the kinetic model fitting for $MAC_{WS\text{-}BrC}$ against stable carbon isotope fingerprinting, during source-to-receptor ageing shows the synchronous trend of atmospheric dynamics, indicating the $\delta^{13}C$ serves as an "ageing clock" and that this kinetic model is applicable to simulate and elucidate the bleaching and transformation of WS-BrC. (iv) the actual bleaching rates—corresponding to a half-life of $MAC_{WS\text{-}BrC}$ of approximately 3 days. The above prevalent photobleaching patterns and aerosol parameter relationships facilitate improved predictions by aerosol modelling (e.g., bleaching rate and source-resolved MAC can be incorporated into the model) and provide

guidance for tailored mitigation actions. To this end, by bridging the influences of sources and atmospheric bleaching on BrC climate, this study suggests models can consider these relatively simple relationships and aerosol parameters to improve predictions of aerosol-induced climate and radiative forcing.

METHODS

The East Asian sampling campaign

The wintertime aerosol pollution campaign was conducted at Beijing, Wuqing (BTH), Shanghai, Haining (YRD), Zhongshan (PRD), Deyang (SC) and Korea Climate Observatory at Gosan (KCOG) in January 2014. The details of sampling sites were described in our previous studies[35,47] (Supplementary Note 1). The sample information and sampling times are provided in Supplementary Table 1. In the same month, seven to ten high-polluted $PM_{2.5}$ samples were collected on pre-combusted quartz-fibre filters in the above sites using $PM_{2.5}$ samplers. At least three filter blanks were collected for each site throughout the campaign.

Measurements of concentrations and isotopes

The filter samples collected at the seven sites were analysed for the concentrations of OC, EC and WS-BrC (for more details on the experiments, see Supplementary Note 5). The concentration measurement protocols were described previously[35–37,39,40,47]. Briefly, EC and OC were measured by a thermal-optical transmission (TOT) analyzer (Sunset Laboratory Inc., Tigard, OR, USA) using the National Institute for Occupational Safety and Health (NIOSH) 5040 method[78]. WS-BrC was extracted by ultra-sonication, centrifugation and filtration of the supernatant and quantified by a high-temperature catalytic oxidation instrument (Shimadzu-TOC-VCPH, Japan)[35–37]. The TC and WS-BrC concentration values were blank-corrected by subtracting an average of the field blanks. The mean relative standard deviation of triplicate analysis was <5% for EC, TC and WS-BrC. Standards and other reference materials frequently calibrated the instruments.

The isotope ($\Delta^{14}C$ and $\delta^{13}C$) measurements were presented in our earlier studies[35–37,39,40,47] (see Supplementary Note 5 for detailed methods). Briefly, synoptic samples (including source-to-receptor samples in E. Asia) with high pollution were selected to isolate the different carbon components (e.g., WS-BrC, EC) and their isotope measurements[35]. For WS-BrC isolation, the Milli-Q water extracts of WS-BrC were freeze-dried and successively to be decarbonated and then transferred into pre-combusted silver capsules for isotope analysis. For EC isolation, a filter area corresponding to at least 60 µg of EC for each sample was subjected to the NIOSH-5040 protocol for oxidation to CO_2, and the produced CO_2 was cryotrapped during the EC combustion phase. Finally, the dried WS-BrC and EC samples in flame-sealed glass ampules were analysed for their natural ^{14}C abundance and $^{13}C/^{12}C$ ratio using accelerator mass spectrometry (AMS) at the US-NSF NOSAMS Facility (Woods Hole, MA, USA) as described previously[35–37,40,47]. The isotope data for the current Jan-2014 E. Asia and other related campaigns in E. and S. Asia are provided in Supplementary Table 4, with a mean and standard deviation of raw data.

Source apportionment

The fractional contribution of fossil fuel sources (f_{fossil}) vs. biomass/biogenic sources (f_{bio}) can be determined using the isotopic mass balance equation:

$$\Delta^{14}C_{sample} = \Delta^{14}C_{fossil} f_{fossil} + \Delta^{14}C_{bio}(1 - f_{fossil}) \quad (1)$$

where, $\Delta^{14}C_{sample}$ represents the measured radiocarbon content of a sample (e.g., WS-BrC, EC) and $\Delta^{14}C_{fossil}$ is −1000‰, since fossil carbon is completely depleted in radiocarbon. Endmembers for contemporary radiocarbon $\Delta^{14}C_{bio}$ fall between +50 and +225‰. In E. Asia of this study, a biomass value of $\Delta^{14}C_{bio} = +112 \pm 60$‰ is suggested and adopted[35,47,49], converting to a variability of <5% in the resulting calculated fraction of biomass using Markov-Chain Monte Carlo (MCMC) techniques. To facilitate the comparison and consistency, the MCMC computation in this study utilized the same source endmembers for $\Delta^{14}C$ and $\delta^{13}C$ (endmembers, see Supplementary Table 3). The calculated fractions of biomass vs. fossil of EC and WS-BrC are available in Supplementary Table 4.

The dual-carbon isotope signatures of EC were used in combination with a MCMC approach to further constrain the relative contributions from three source classes: biomass (f_{bio}), coal (f_{coal}) and liquid fossil fuel ($f_{liq\ fossil}$)[49].

$$\begin{pmatrix} \Delta^{14}C\_sample \\ \delta^{13}C\_sample \\ 1 \end{pmatrix} = \begin{pmatrix} \Delta^{14}C\_bio & \Delta^{14}C\_liq\ fossil & \Delta^{14}C\_coal \\ \delta^{13}C\_bio & \delta^{13}C\_liq\ fossil & \delta^{13}C\_coal \\ 1 & 1 & 1 \end{pmatrix} \cdot \begin{pmatrix} f\_bio \\ f\_liq\ fossil \\ f\_coal \end{pmatrix} \quad (2)$$

Where f denotes the fractional contribution from a given source, sample denotes the value of the analysed field sample, and the other isotope values are source signatures ('bio', 'liq fossil' and 'coal' corresponding to biomass/biogenic, liquid fossil fuel and coal, respectively). The last row ensures the mass-balance principle. The Bayesian MCMC computed source apportionments (biomass, coal and liquid fossil) of EC using raw isotope ($\Delta^{14}C$ and $\delta^{13}C$) data reported for current Jan-2014 E. Asian campaign and other E. and S. Asian sites in previous literature, are provided in Supplementary Table 5 (key results for comparison are shown in Fig. 3).

Measurements of the optical properties of WS-BrC

The following suggested equation was applied to convert the absorption of solution WS-BrC to the absorption coefficient of ambient particle WS-BrC[38,44]:

$$b_{abs} = (A_{365} - A_{700}) \frac{V_w \cdot \ln(10)}{V_a \cdot L} \quad (3)$$

where V_W is the volume of water for filter sample extraction, V_a is the volume of air sampled through the extracted subsample, L is the light path length (1 cm, for the currently used quartz cuvettes), A_{365} and A_{700} are the measured base-10 absorbance of the liquid extract (assuming that the scattering contribution to extinction is low) at 365 (averaged between 360 and 370 nm) and 700 nm (averaged between 695 and 705 nm, these wavelengths represent background).

The light absorption of WS-BrC was measured from water extracts using a Hitachi U2010 spectrophotometer, with scanning wavelength from 190 to 1100 nm. The mass absorption cross-section (MAC, $m^2\ g^{-1}$) was computed as:

$$MAC_{365} = \frac{b_{abs(365)}}{[WSBrC]} \quad (4)$$

where $b_{abs(365)}$ is the light-absorption coefficient (Mm^{-1}) at 365 nm, [WS-BrC] is the solution concentration of WS-BrC. The $MAC_{WS\text{-}BrC}$ is presented at 365 nm to enable comparison with previous studies[36–46,55–57,59,60]. The wavelength (λ) dependence of the WS-BrC absorption was investigated by fitting an absorption Ångström exponent (AÅE) using the following relation:

$$\frac{A(\lambda_1)}{A(\lambda_2)} = \left(\frac{\lambda_2}{\lambda_1}\right)^{AÅE} \quad (5)$$

AÅE (shown in Supplementary Fig. 9) was fitted within the range 330–400 nm to avoid interference from light-absorbing inorganic components such as nitrate[38].

East or South Asia maintained their own constant source contribution

The isotopic composition of the aerosol pollution stayed relatively constant over the course of the study, as exemplified by: (i) In E. Asia, the EC isotope signals in January of 2013 and 2014 BTH and Jan-2014 Beijing were similar ($\delta^{13}C$: –23.5 to –24.4‰; $\Delta^{14}C$: –710 to –772‰). Our MCMC results show that EC in Beijing and BTH were dominated by fossil coal (from 53 to 56%) with similar shares of three main sources (that is, biomass, coal and liquid fossil) in January 2014 (see Fig. 3a). A similar source share to EC-BTH was observed in Jan-2013, with coal burning up to 62 ± 9% (Supplementary Table 5). The EC in megacity Shanghai (Jan-2014), other sites in YRD (Jan-2013; a nearby site to Shanghai) and PRD (Jan-2013) showed similar isotopes and source shares, mainly from liquid fossil fuel (Fig. 3a, Supplementary Table 5). This similarity of ^{14}C and thus sources is also reflected in WS-BrC[35,46,47,49]. The fraction biomass of Beijing-WS-BrC from this Jan-2014 campaign (f_{bio}, 44 ± 4%) is identical to that of Jan-2013 (f_{bio}, 43 ± 3%ref. [46]). Moreover, very similar isotope signatures were observed during this study (f_{bio}, 50 ± 8%; $\delta^{13}C$, –22.8 ± 0.2‰) compared to 2011 (f_{bio}, ~50%; $\delta^{13}C$, –23.0 ± 0.7‰) at KCOGref. [36], which is a large regional footprint and receptor intercepted the E. Asian outflow. Our results show that the f_{bio} of EC (WS-BrC) is likely in the range of approximately 20–33% (43–50%), respectively, in Jan-2014 E. Asia, with tentative uncertainty of ~5–10%. (ii) In contrast to E. Asia, our MCMC calculations (using the previously observed isotope data) show that EC (f_{bio}, 50–59%) and WS-BrC (f_{bio}, 79–87%) in S. Asia were dominated by biomass in both source (e.g., megacity Delhi) and regionally-footprint ocean-background site (Fig. 3b; for isotope data, see Supplementary Table 4). The emission areas and remote sites shared similar fractional source contributions to EC in the same year (e.g., BCOB and MCOH 2016; the isotope and MAC data from these 2016 campaigns were used for comparison in this study) as in megacities 2011 Delhi and 2013/14 Dhaka, and at the same site in different years (e.g., 2012 and 2016 MCOH) (see Fig. 3b; refs. therein). Generally, the observed f_{bio} of WS-BrC was ~20–30% higher than that of EC; for example, f_{bio} (Delhi 2011) of WS-BrC and EC were 79% and 50%, respectively, f_{bio} (MCOH 2012) of WS-BrC and EC were 87% and 59%, respectively. It is likely because biomass burning produced more water-soluble carbon aerosols (aerosol emission factor) than, for example, vehicle emissions did[12,19,54]. Thus, the similar source contributions to EC and WS-BrC in S. Asia again suggest that, over the comparison periods, it is also little variability for their sources in S. Asia.

Test the impact of SOA vs. photochemical bleaching on light absorption

Using a limiting case as an assumption, we assume that: (i) primary WS-BrC (MAC and amount) remains unchanged without any reactions, evaporation and condensation/partition during source-to-receptor transport; (ii) secondary WS-BrC (using OC instead OA) is formed in the aged KCOG aerosols; (iii) secondary WS-BrC accounts for ~30% (or 50%) of total WS-BrC in receptor KCOG. To achieve an approximately two-fold reduction of $MAC_{WS\text{-}BrC}$ from the inland site (e.g., $MAC_{Beijing} = 1.7 \pm 0.2\ m^2\ g^{-1}$) to the ocean background site (i.e., $MAC_{KCOG} = 0.89 \pm 0.28\ m^2\ g^{-1}$), the calculated $MAC_{(secondary\ WS\text{-}BrC)}$ is a negative value –1 (or close to 0) based on the mass balance equation ($MAC_{KCOG} = MAC_{Beijing} \cdot 0.7 + MAC_{(secondary\ WS\text{-}BrC)} \cdot 0.3 = 0.89\ m^2\ g^{-1}$). This is controversial since most past studies have indicated that SOA also has absorptive capacity. That means there must be large atmospheric bleaching of WS-BrC during long-range oversea transport.

Calculation of the WS-BrC bleaching rate during oversea transport

During the dispersal of East Asian haze, the bleaching rate of WS-BrC was calculated by the following empirical formula[39]:

$$MAC_{KCOG\text{-}WS\text{-}BrC} = MAC_{Beijing\text{-}WS\text{-}BrC} \cdot e^{-kt} \quad (6)$$

Where k (day^{-1}) is the first-order bleaching rate and t (day) is the mean synoptic air mass transport time for the corresponding outflow samples intercepted at the regional receptor KCOG from northern E. Asian continent (i.e., BTH/Beijing) to KCOG. On average, air mass transport times were estimated based on the HYSPLIT BTs analysis (e.g., Table 1, Supplementary Figs. 5 and 6). The half-life for a first-order degradation (here refers to bleaching) of water-soluble BrC is always Ln (2)/k.

Estimation of the relative solar absorption by WS-BrC versus BC

The fraction (f) solar energy absorbed by WS-BrC relative to BC was calculated as the wavelength-integrated product of the solar spectrum and WS-BrC absorption divided by the analogous integral for BC (for measurement of MAC_{EC}, see Supplementary Note 6; for f calculation, see Supplementary Note 7; for MAC_{EC} results, see Supplementary Fig. 10). Supplementary Figs. 11–14 showed the tropospheric solar absorption spectra of WS-BrC and BC against wavelength (range of 300–800 nm) at ground level over E. Asia. The calculated average fractions (f) of the total direct absorbance by WS-BrC relative to BC varied significantly from 3 ± 1.0% to 21 ± 9% over E. Asia (Supplementary Fig. 15, Supplementary Table 7; for relative absorption model of WS-BrC/BC, assumptions and calculation details, see Supplementary Note 7). This calculation aims to broadly evaluate the solar spectrum integrated relative absorbance of WS-BrC and EC at a ground-level situation over E. Asia. However, the calculation based on the ground-level observation might be different when integrated over a vertical column. One reason is that the vertical distributions of carbonaceous aerosols need a site-specific evaluation.

The ratios of total absorbance of WS-BrC to BC are dominated by two factors: the light-absorbing efficiency (MAC) by WS-BrC and the concentration ratio of WS-BrC to EC at different sites. Compared to the regional sites (BTH and YRD), the relatively lower fraction f (3.1 ± 1.0, or 6.2 ± 1.6) observed at source sites (e.g., Beijing) was due to relatively lower concentration ratios of WS-BrC to EC. On the other hand, the highest mass ratios (~2 times greater than that of the Beijing site) of WS-BrC/EC at the regional receptor KCOG led to the highest fractions (10.5 ± 4.3, 21.0 ± 8.6) of solar radiation absorbed by WS-BrC relative to EC (Supplementary Fig. 15). We note that the strongly wavelength-dependent WS-BrC exhibits a rapid increase in tropospheric solar absorption at the shorter wavelength (e.g., 300–500 nm) and the relative contribution relative to BC can be up to more than 100% in these wavelengths (Supplementary Figs. 16 and 17).

Additional information about concentration measurements of carbonaceous aerosols, synoptic weather patterns, AOD and BTs analysis are provided in Supplementary Note 8. Appendix for the abbreviations is shown in Supplementary Note 9.

DATA AVAILABILITY

The observational data that support the findings of this study are provided in SI, and all the datasets are archived on the open-access Zenodo repository (https://zenodo.org/record/8146770) and will also be publicly available at the Stockholm University Bolin Center Database website (http://bolin.su.se/data/).

CODE AVAILABILITY

The sampling of the posterior distribution of the MC formulation can be done by using a method available at http://www.r-project.org/conferences/DSC-2003/ using

rjags (http://cran.rproject.org/web/packages/rjags/index.html), implemented in the freely available R software (http://www.r-project.org/).

Received: 18 December 2022; Accepted: 21 July 2023;
Published online: 29 July 2023

REFERENCES

1. Klimont, Z. et al. Global anthropogenic emissions of particulate matter including black carbon. *Atmos. Chem. Phys.* **17**, 8681–8723 (2017).
2. Gustafsson, Ö. & Ramanathan, V. Convergence on climate warming by black carbon aerosols. *Proc. Natl Acad. Sci. USA* **113**, 4243–4245 (2016).
3. Ramanathan, V. & Carmicheal, G. Global and regional climate changes due to black carbon. *Nat. Geosci.* **1**, 221–227 (2008).
4. Seinfeld, J. Black carbon and brown clouds. *Nat. Geosci.* **1**, 15–16 (2008).
5. Ebenstein, A. et al. New evidence on the impact of sustained exposure to air pollution on life expectancy from China's Huai River Policy. *Proc. Natl Acad. Sci. USA* **113**, 10384–10389 (2016).
6. Szopa, S. et al. Short-lived climate forcers. In *IPCC Climate Change 2021: The Physical Science Basis. Contribution of Working Group I to the Sixth Assessment Report of the Intergovernmental Panel on Climate Change,* IPCC Chapter 6, 817–922 (Cambridge University Press, 2021).
7. Laskin, A., Laskin, J. & Nizkorodov, S. A. Chemistry of atmospheric brown carbon. *Chem. Rev.* **115**, 4335–4382 (2015).
8. Alexander, D. T. L. et al. Brown carbon spheres in East Asia outflow and their optical properties. *Science* **321**, 833–836 (2008).
9. Zhang, Y. et al. Top-of-atmosphere radiative forcing affected by brown carbon in the upper troposphere. *Nat. Geosci.* **10**, 486–489 (2017).
10. Chung, C. E., Ramanathan, V. & Decremer, D. Observational constrained estimates of carbonaceous aerosol radiative forcing. *Proc. Natl Acad. Sci. USA* **109**, 11624–11629 (2012).
11. Bond, T. C. & Bergstrom, R. W. Light absorption by carbonaceous particles: an investigative review. *Aerosol Sci. Technol.* **40**, 27–67 (2006).
12. Cappa, C. D. et al. Biomass-burning-derived particles from a wide variety of fuels —Part 2: Effects of photochemical aging on particle optical and chemical properties. *Atmos. Chem. Phys.* **20**, 8511–8532 (2020).
13. Saleh, R. et al. Brownness of organics in aerosols from biomass burning linked to their black carbon content. *Nat. Geosci.* **7**, 647–650 (2014).
14. Zhong, M. & Jang, M. Dynamic light absorption of biomass burning organic carbon photochemically aged under natural sunlight. *Atmos. Chem. Phys.* **14**, 1517–1525 (2014).
15. Forrister, H. et al. Evolution of brown carbon in wildfire plumes. *Geophys. Res. Lett.* **42**, 4623–4630 (2015).
16. Ni, H. et al. Brown carbon in primary and aged coal combustion emission. *Environ. Sci. Technol.* **47**, 6349–6357 (2021).
17. Tang, J. et al. Molecular compositions and optical properties of dissolved brown carbon in biomass burning, coal combustion, and vehicle emission aerosols illuminated by excitation–emission matrix spectroscopy and Fourier transform ion cyclotron resonance mass spectrometry analysis. *Atmos. Chem. Phys.* **20**, 2513–2532 (2020).
18. Liu, D. et al. Evolution of aerosol optical properties from wood smoke in real atmosphere influenced by burning phase and solar radiation. *Environ. Sci. Technol.* **47**, 6349–6357 (2021).
19. McMeeking, G. R. et al. Impacts of nonrefractory material on light absorption by aerosols emitted from biomass burning. *J. Geophys. Res. Atmos.* **119**, 12272–12286 (2014).
20. Saleh, R. et al. Absorptivity of brown carbon in fresh and photo-chemically aged biomass-burning emissions. *Atmos. Chem. Phys.* **13**, 7683–7693 (2013).
21. Wong, J. P. S., Nenes, A. & Weber, R. J. Changes in light absorptivity of molecular weight separated brown carbon due to photolytic aging. *Environ. Sci. Technol.* **51**, 8414–8421 (2017).
22. Kirchstetter, T. W. et al. Evidence that the spectral dependence of light absorption by aerosols is affected by organic carbon. *J. Geophys. Res. Atmos.* **109**, D21208 (2004).
23. Palm, B. B. et al. Quantification of organic aerosol and brown carbon evolution in fresh wildfire plumes. *Proc. Natl Acad. Sci. USA* **117**, 29469–29477 (2020).
24. Kleinman, L. I. et al. Rapid evolution of aerosol particles and their optical properties downwind of wildfires in the western US. *Atmos. Chem. Phys.* **20**, 13319–13341 (2020).
25. Ortega, A. M. et al. Secondary organic aerosol formation and primary organic aerosol oxidation from biomass-burning smoke in a flow reactor during FLAME-3. *Atmos. Chem. Phys.* **13**, 11551–11571 (2013).
26. Bruns, E. A. et al. Identification of significant precursor gases of secondary organic aerosols from residential wood combustion. *Sci. Rep.* **6**, 27881 (2016).
27. Wang, Q. et al. Wintertime optical properties of primary and secondary brown carbon at a regional site in the North China Plain. *Environ. Sci. Technol.* **53**, 12389–12397 (2019).
28. Gilardoni, S. et al. Direct observation of aqueous secondary organic aerosol from biomass-burning emissions. *Proc. Natl Acad. Sci. USA* **113**, 10013–10018 (2016).
29. Cubison, M. J. et al. Effects of aging on organic aerosol from open biomass burning smoke in aircraft and laboratory studies. *Atmos. Chem. Phys.* **11**, 12049–12064 (2011).
30. Akagi, S. K. et al. Evolution of trace gases and particles emitted by a chaparral fire in California. *Atmos. Chem. Phys.* **12**, 1397–1421 (2012).
31. Garofalo, L. A. et al. Emission and evolution of submicron organic aerosol in smoke from wildfires in the western United States. *ACS Earth Space Chem.* **3**, 1237–1247 (2019).
32. Liu, X. et al. Agricultural fires in the southeastern U.S. during SEAC4RS: Emissions of trace gases and particles and evolution of ozone, reactive nitrogen, and organic aerosol. *J. Geophys. Res. Atmos.* **121**, 7383–7414 (2016).
33. Wang, X. et al. Exploring the observational constraints on the simulation of brown carbon. *Atmos. Chem. Phys.* **18**, 635–653 (2018).
34. June, N. A. et al. Spatial and temporal variability of brown carbon in the United States: implications for direct radiative effects. *Geophys. Res. Lett.* **47**, e2020GL090332 (2020).
35. Fang, W. et al. Divergent evolution of carbonaceous aerosols during dispersal of East Asian haze. *Sci. Rep.* **7**, 10422 (2017).
36. Kirillova, E. N., Andersson, A., Han, J., Lee, M. & Gustafsson, Ö. Sources and light absorption of water-soluble organic carbon aerosols in the outflow from northern China. *Atmos. Chem. Phys.* **14**, 1413–1422 (2014).
37. Bosch, C. et al. Source-diagnostic dual-isotope composition and optical properties of water-soluble organic carbon and elemental carbon in the South Asian outflow intercepted over the Indian Ocean. *J. Geophys. Res. Atmos.* **119**, 11743–11759 (2014).
38. Cheng, Y. et al. Mass absorption efficiency of elemental carbon and water-soluble organic carbon in Beijing, China. *Atmos. Chem. Phys.* **11**, 11497–11510 (2011).
39. Dasari, S. et al. Photochemical degradation affects the light absorption of water-soluble brown carbon in the South Asian outflow. *Sci. Adv.* **5**, eaau8066 (2019).
40. Kirillova, E. N. et al. Water-soluble organic carbon aerosols during a full New Delhi winter: isotope-based source apportionment and optical properties. *J. Geophys. Res. Atmos.* **119**, 3476–3485 (2014).
41. Yan, C. et al. Chemical characteristics and light-absorbing property of water-soluble organic carbon in Beijing: Biomass burning contributions. *Atmos. Environ.* **121**, 4–12 (2015).
42. Du, Z. et al. A yearlong study of water-soluble organic carbon in Beijing II: light absorption properties. *Atmos. Environ.* **89**, 235–241 (2014).
43. Kirillova, E. N. et al. ^{13}C- and ^{14}C-based study of sources and atmospheric processing of water-soluble organic carbon (WSOC) in South Asian aerosols. *J. Geophys. Res. Atmos.* **118**, 614–626 (2013).
44. Hecobian, A. et al. Water-soluble organic carbon material and the light-absorption characteristic of aqueous extracts measured over the Southeastern United States. *Atmos. Chem. Phys.* **10**, 5965–5977 (2010).
45. Liu, J. et al. Size-resolved measurements of brown carbon in water and methanol extracts and estimates of their contribution of ambient fine-particle light absorption. *Atmos. Chem. Phys.* **13**, 12389–12404 (2013).
46. Yan, C. et al. Important fossil source contribution to brown carbon in Beijing during winter. *Sci. Rep.* **7**, 43182 (2017).
47. Fang, W. et al. Dual-isotope constraints on seasonally resolved source fingerprinting of black carbon aerosols in sites of the four emission hot spot regions of China. *J. Geophys. Res. Atmos.* **123**, 11735–11747 (2018).
48. Bikkina, S. et al. Air quality in megacity Delhi affected by countryside biomass burning. *Nat. Sustain.* **2**, 200–205 (2019).
49. Andersson, A. et al. Regionally-varying combustion sources of the January 2013 severe haze events over eastern China. *Environ. Sci. Technol.* **49**, 2038–4496 (2015).
50. Kroll, J. H. et al. Carbon oxidation state as a metric for describing the chemistry of atmospheric organic aerosol. *Nat. Chem.* **3**, 133–139 (2011).
51. Andersson, A. A model for the spectral dependence of aerosol sunlight absorption. *ACS Erath Space Chem.* **1**, 533–539 (2017).
52. Salam, A. et al. Wintertime air quality in Megacity Dhaka, Bangladesh strongly affected by influx of black carbon aerosols from regional biomass burning. *Environ. Sci. Technol.* **55**, 12243–12249 (2021).
53. Dasari, S. et al. Source quantification of south Asian black carbon aerosols with isotopes and modeling. *Environ. Sci. Technol.* **54**, 11771–11779 (2020).
54. Miyazaki, Y. et al. Time-resolved measurements of water-soluble organic carbon in Tokyo. *J. Geophys. Res.* **111**, D23206 (2006).

55. Li, M. et al. Abundance and light absorption properties of brown carbon emitted from residential coal combustion in China. *Environ. Sci. Technol.* **53**, 595–603 (2019).
56. Park, S. S. & Yu, J. Chemical and light absorption properties of humic-like substances from biomass burning emissions under controlled combustion experiments. *Atmos. Environ.* **136**, 114–122 (2016).
57. Cheng, Y. et al. Strong impacts of legitimate open burning on brown carbon aerosol in northeast China. *Environ. Sci. Technol. Lett.* **8**, 732–738 (2021).
58. Moschos, V. et al. Source-specific light absorption by carbonaceous components in the complex aerosol matrix from yearly filter-based measurements. *Atmos. Chem. Phys.* **21**, 12809–12833 (2021).
59. Zhang, X., Lin, Y. H., Surratt, J. D. & Weber, R. J. Sources, composition and absorption Angstrom exponent of light-absorbing organic components in aerosol extracts from the Los Angeles Basin. *Environ. Sci. Technol.* **47**, 3685–3693 (2013).
60. Zhang, X. et al. Light-absorbing soluble organic aerosol in Los Angeles and Atlanta: a contrast in secondary organic aerosol. *Geophys. Res. Lett.* **38**, L21810 (2011).
61. Pavuluri, C. M. & Kawamura, K. Enrichment of ^{13}C in diacids and related compounds during photochemical processing of aqueous aerosols: new proxy for organic aerosols aging. *Sci. Rep.* **6**, 36467 (2016).
62. Aggarwal, S. G. & Kawamura, K. Molecular distributions and stable carbon isotopic compositions of dicarboxylic acids and related compounds in aerosols from Sapporo, Japan: implications for photochemical aging during long-range atmospheric transport. *J. Geophys. Res. Atmos.* **113**, D14301 (2008).
63. Irei, S. et al. Stable carbon isotope ratio of secondary particulate organic matter formed by photooxidation of toluene in indoor smog chamber. *Atmos. Environ.* **45**, 856–862 (2011).
64. Anderson, R. S. et al. Carbon kinetic isotope effects in the gas-phase reactions of aromatic hydrocarbons with the OH radical at 296 ± 4 K. *Geophys. Res. Lett.* **31**, L15108 (2004).
65. Fang, W. et al. Thermal desorption/Tunable vacuum-ultraviolet time-of-flight photoionization aerosol mass spectrometry for investigating secondary organic aerosols in chamber experiments. *Anal. Chem.* **83**, 9024–9032 (2011).
66. Fang, W. et al. Measurements of secondary organic aerosol formed from OH-initiated photo-oxidation of isoprene using on-line photoionization aerosol mass spectrometry. *Environ. Sci. Technol.* **46**, 3898–3904 (2012).
67. Fang, W. et al. Online analysis of secondary organic aerosols from OH-initiated photooxidation and ozonolysis of α-pinene, β-pinene, Δ^3-carene and d-limonene by thermal desorption–photoionisation aerosol mass spectrometry. *Environ. Chem.* **14**, 75–90 (2017).
68. Irei, S. et al. Laboratory studies of carbon kinetic isotope effects on the production mechanism of particulate phenolic compounds formed by toluene photooxidation: a tool to constrain reaction pathways. *J. Phys. Chem. A.* **119**, 5–13 (2015).
69. Fisseha, R. et al. Stable carbon isotope composition of secondary organic aerosol from beta-pinene oxidation. *J. Geophy. Res. Atmos.* **114**, D02304 (2009).
70. Lambe, A. T. et al. Relationship between oxidation level and optical properties of secondary organic aerosol. *Environ. Sci. Technol.* **47**, 6349–6357 (2013).
71. Adler, G. et al. Chemical, physical, and optical evolution of biomass burning aerosols: a case study. *Atmos. Chem. Phys.* **11**, 1491–1503 (2011).
72. Lee, H. J. et al. Effect of solar radiation on the optical properties and molecular composition of laboratory proxies of atmospheric brown carbon. *Environ. Sci. Technol.* **48**, 10217–10226 (2014).
73. Romonosky, D. E. et al. Effective absorption cross sections and photolysis rates of anthropogenic and biogenic secondary organic aerosols. *Atmos. Environ.* **130**, 172–179 (2016).
74. Hems, R. F. et al. Aging of atmospheric brown carbon aerosol. *ACS Earth Space Chem.* **5**, 722–748 (2021).
75. Lin, P. et al. Molecular characterization of brown carbon in biomass burning aerosol particles. *Environ. Sci. Technol.* **50**, 11815–11824 (2016).
76. Zhao, R. et al. Photochemical processing of aqueous atmospheric brown carbon. *Atmos. Chem. Phys.* **15**, 6087–6100 (2015).
77. Hems, R. F. & Abbatt, J. P. D. Aqueous phase photo-oxidation of brown carbon nitrophenols: reaction kinetics, mechanism, and evolution of light absorption. *ACS Earth Space Chem.* **2**, 225–234 (2018).
78. Birch, M. E. & Cary, R. A. Elemental carbon-based method for monitoring occupational exposures to particulate diesel exhaust. *Aerosol Sci. Technol.* **25**, 221–241 (1996).

ACKNOWLEDGEMENTS

This work was supported by a combination of Swedish, Chinese, EU and South Korean funding sources. We acknowledge the Swedish Research Council (FORMAS grant no. 942-2015-1061 and VR Distinguished Professorship grant to Ö. G., no. 2017-01601). W.F. acknowledges the start-up funding from East China Normal University and EU financial support from Marie Curie individual fellow programme (H2020-MSCA-IF-GA-2014-659529). K.D. acknowledges the support from the Strategic Priority Research Program (B) of the Chinese Academy of Sciences (XDB05060200) for aerosol sampling. S.-W.K. was supported by the Basic Science Research Program through the National Research Foundation of Korea (NRF), funded by the Ministry of Education (2017R1D1A1B06032548).

AUTHOR CONTRIBUTIONS

W.F., A.A. and Ö.G. conceived the project. K.D., Ö.G., M.L. and M.Z. designed the sampling project. W.F. analysed the samples, performed the calculations, conceived the models, and produced the figures. W.F., A.A. and Ö.G. interpreted the data. W.F. drafted the manuscript, and A.A. and Ö.G. revised the paper. All co-authors reviewed the paper.

FUNDING

Open access funding provided by Stockholm University.

COMPETING INTERESTS

The authors declare no competing interests.

ADDITIONAL INFORMATION

Supplementary information The online version contains supplementary material available at https://doi.org/10.1038/s41612-023-00438-8.

Correspondence and requests for materials should be addressed to Wenzheng Fang or Örjan Gustafsson.